

MARLIN: A Co-Design Methodology for Approximate Reconfigurable Inference of Neural Networks at the Edge

Flavia Guella¹, *Student Member, IEEE*, Emanuele Valpreda¹, *Student Member, IEEE*,
Michele Caon¹, *Student Member, IEEE*, Guido Maserà¹, *Senior Member, IEEE*,
and Maurizio Martina¹, *Senior Member, IEEE*

Abstract—The optimization of neural networks (NNs) is necessary to enable their deployment on energy-constrained devices. State-of-the-art methods leverage approximate multipliers to execute NNs reducing the inference energy without heavily affecting the accuracy. However, previous works usually require a specialized hardware accelerator and are limited to fixed multipliers or reconfigurable ones with few approximation levels. This paper introduces MARLIN, a framework to deploy layerwise approximate NNs on PULP, a microcontroller with a RISC-V core. A multiplier architecture, with runtime selection of 256 approximation levels, is developed and integrated into the PULP cluster cores, enabling runtime configuration through control status register (CSR) instructions embedded within the code. The PULP toolchain is adapted to incorporate the approximation level selection within the instruction flow seamlessly. MARLIN leverages the genetic algorithm NSGA-II to search for the best configurations among thousands of approximate NNs. The framework is validated by simulating an approximate NN trained with the MNIST dataset on PULP. Moreover, MARLIN is used to optimize and approximate six ResNet models trained with the CIFAR-10 dataset. In particular, for ResNet-56, the most complex NN used in the experiments, the multiplication energy is reduced by 23.9% while retaining 99% of the accuracy of the exact model.

Index Terms—Approximate computing, neural networks, RISC-V, hardware acceleration, reconfigurable computing.

I. INTRODUCTION

IN RECENT years, there has been an increasing necessity to include neural networks (NNs) in embedded systems to deliver more advanced functionalities. Nonetheless, NNs superior task accuracy comes at the cost of high computational complexity and memory requisites, thereby presenting

challenges in deploying them on energy-constrained devices, such as microcontrollers (MCUs) [1], [2]. Over the past decade, dedicated hardware accelerators [3], [4], [5], [6], [7], [8], [9] have been developed to optimize energy efficiency and throughput during inference by reducing the data movement and the cost of arithmetic operations. The latter usually accounts for around a fourth of the total inference energy, as the convolutional and fully connected layers of NNs involve millions of multiplications and additions [10]. Nowadays, quantization-aware training can reduce the bitwidth of NN models to 8 bits or below with little or no loss in accuracy [3], [11], [12], [13]. It lowers the amount of memory traffic and the computational cost, allowing the deployment of NNs on low-power devices with no support for floating-point arithmetic. Layer-wise quantization leverages the different degrees of robustness and tolerance to error introduction of NN layers. Therefore, a runtime reconfigurable multiplier supporting operands with different bitwidths is necessary to leverage mixed-precision and layer-wise quantization [3], [4], [11], [12]. Similarly to quantization, approximation is another co-design technique mainly aimed at reducing the inference energy [14]. The basic idea is to reduce computational complexity and cost using operators that produce inexact results. However, as already pointed out, there is high variability in the sensitivity of single layers inside the same model and among different models. Therefore, designing a multiplier with different approximation levels is fundamental to ensure flexibility and adaptability. Several strategies have been explored in the literature to design hardware supporting layer-wise approximate NNs [15], [16], [17], leveraging retraining or parameters fine-tuning to reduce the accuracy degradation. However, previous works rely on specialized accelerators and support very few approximation levels [17], [18], limiting the possibility of finding the optimal error-accuracy trade-off; other works use several non-reconfigurable multipliers instances in the accelerator's systolic array [15], [19], [20]. The latter approach increases the area overhead and prevents the same hardware from executing NNs with different parameters or NNs with different model architectures with the same energy efficiency or accuracy. Since Internet of Things (IoT) devices have limited area and power budgets [1], [2] and must be able to adapt to different workloads and performance targets, it is

Manuscript received 14 September 2023; revised 7 December 2023 and 14 January 2024; accepted 10 February 2024. Date of publication 27 February 2024; date of current version 30 April 2024. This work was supported in part by the Key Digital Technologies Joint Undertaking and Its Members through the TRISTAN Project Under Grant 101095947 and in part by the MUR—M4C2 1.5 of PNRR funded by the European Union—NextGenerationEU through the NODES Project under Grant ECS00000036. This article was recommended by Associate Editor Y. Tang. (Flavia Guella, Emanuele Valpreda, and Michele Caon contributed equally to this work.) (Corresponding authors: Flavia Guella; Emanuele Valpreda.)

The authors are with the Department of Electronics and Telecommunications, Politecnico di Torino, 10129 Turin, Italy (e-mail: flavia.guella@polito.it; emanuele.valpreda@polito.it).

Color versions of one or more figures in this article are available at <https://doi.org/10.1109/TCSI.2024.3365952>.

Digital Object Identifier 10.1109/TCSI.2024.3365952

necessary to adopt a layer-wise approximation strategy that relies on a single multiplier offering several accuracy levels. Moreover, the architecture using this multiplier should be programmable and reconfigurable to support the deployment of different NNs, reusing the same hardware as efficiently as possible without requiring a redesign or recall of the IoT device. Such flexibility allows choosing which NN is suited for a particular scenario, prioritizing the battery life of the edge device or the accuracy of the predictions.

In this work, we present MARLIN, an automated layer-wise approximation co-design methodology that enables searching for the optimal energy-accuracy trade-off and deploying approximate NNs on a hardware accelerator. We leverage a runtime-reconfigurable parallel tree multiplier featuring 256 error levels, assigning low-power inaccurate multiplier configurations to layers with high error resilience and more accurate, albeit less efficient, setup to layers with low error tolerance. Moreover, we search for different network-level approximate configurations, i.e., NNs with the same model architecture but a different layer-wise approximation and, consequently, energy-accuracy trade-off, supporting different workload priorities. In order to rapidly deploy an approximate NN and prove the portability of this method to a known open-source hardware, we selected the PULP MCU [21] as the target IoT platform with RI5CY [22], a RISC-V core. The search of the approximate NNs configuration is done with a non-dominated sorting genetic algorithm (NSGA-II) [23]. This procedure is automated and executed offline, before the NN is mapped to any specific hardware. The configuration of the arithmetic units, using the search results, is done online. The contributions of this work are summarized as follows:

- A layer-wise approximation strategy that reduces the energy of arithmetic operations while retaining the original task accuracy, applicable to any NN topology with convolutional and fully connected layers, with no modification to the model architecture. During the optimization process, relying on NSGA-II, approximate NNs are evaluated by their error resilience and energy, assigning to each layer a different multiplier configuration.
- A runtime reconfigurable signed multiplier supporting 256 approximation levels.
- The post-synthesis simulation of the proposed methodology on a RI5CY core, adapted to include the proposed approximate multiplier, supporting the runtime selection of the accuracy. The entire deployment process of the approximate NN is automated and requires no specific knowledge of the optimization method.
- The code used in this work, the experimental data, and the instructions to replicate the results presented in this paper are available at <https://github.com/vlsi-lab/MARLIN>

This article is organized as follows: Section II introduces a background on NN accelerators and relevant works on approximate inference, discussing the differences with MARLIN, Section III details the co-design framework, the search strategy, the multiplier design, and the modified PULP-toolchain, Section IV presents the results, a comparison with the state-of-the-art, and discusses the trade-offs of reconfigurable approximate computing, and Section V summarizes the paper.

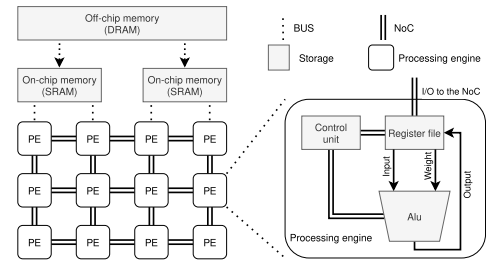


Fig. 1. Generic high-level model of a hardware accelerator for NN inference.

II. BACKGROUND AND RELATED WORKS

A. Hardware Accelerators and Mapping

NN accelerators are typically based on a hardware architecture that comprises a memory hierarchy and an array of interconnected processing engines (PEs) [4], [7], [8], [9], [10], similar to the one depicted in Figure 1. The memory hierarchy usually comprises the system’s main memory (off-chip), global buffers (on-chip), and the registers within the processing engines. The off-chip and on-chip memories are connected through the system’s bus, whereas the PEs communicate through a network-on-chip. The execution of a NN is scheduled with a dedicated mapper that generates the instructions and partitions the resources, minimizing the energy and latency associated with the data movement. The complete cost of a multiplication considered by a mapper includes the energy and latency required to read all the operands, move them through the memory hierarchy, compute and store the result [9], [10], [24], [25]. The mappers used in [7], [8], and [9] can be compared to the compilers used to generate machine code for processors such as RI5CY [22], which purpose is to optimize the performance and resource usage. The approximation methodology described in Section III is orthogonal to the mapping process as it only modifies the energy associated with the arithmetic operations and not the data movement. In [24] a tool that predicts the energy of approximate NN with a mapper based on [10] is presented validating the assumption that approximate computing only modifies the arithmetic energy without affecting the data movement. Therefore, MARLIN does not influence the mapping and could be easily integrated in [7], [8], and [9] similarly to what has been done for DORY in Section III-E, as discussed in Section IV-D. Alternative hardware architectures for energy efficient NN inference at the edge are MCUs. ISA extensions and dedicated dot-product units inserted in the RISC-V pipeline are used in [5] and [6], whereas in [26] a low-power neural processing unit is connected to the MCU through the bus. In this work, we selected PULP [5] as the target platform, a MCU-based low-power computing platform with a host CPU relying on the RI5CY or zero-riscy cores and equipped with a multi-core programmable cluster. The motivation of using PULP is twofold: the RTL and the toolchain are open-source and well documented [21], and, being a MCU-based platform, PULP truly represents a low-power IoT device with strict resource constraints [2]. Additionally, PULP is selected to produce a prototype that can be shared and adapted, without limiting the compatibility of this methodology to the PULP platform, as highlighted by the

fact that the layer-wise approximation strategy of Section III-B and the deployment process of Section III-E do not have any hardware dependencies except the multiplier. The PULP project includes libraries and tools to easily export a NN model written in PyTorch to C code compatible with the MCU. The MARLIN framework includes modified versions of the RISCY core and software tools, adapted to include the approximation level selection through control status register (CSR) instructions, whose generation and compilation are added to the original PULP toolchain.

B. Approximate Neural Networks

In [19], 600 non-reconfigurable approximate multipliers are tested with a multi-layer perceptron for MNIST and LeNet-5 for the Street View House Numbers dataset. Each approximate neural network is executed using one of the 600 multipliers for every convolutional layer following five retraining steps, thus generating 600 different sets of weights for each model. In [16] and [27] it is suggested that hardware-aware retraining, while being a time-consuming, resource-intensive strategy, can mitigate the effect of approximation. Mrazek et al. in [15] present ALWANN, a framework for the approximation of NNs where the assignment of each layer to an approximate multiplier, among the eight-bit ones in EvoApproxLib [28], is performed through the multi-objective genetic algorithm NSGA-II. The parameters of each approximate NN are fine-tuned (updated w.r.t. the starting model) without retraining. Therefore, for each approximate configuration, a new set of weights must be used for each convolutional layer. Similarly, Jain et al. in [20] present a methodology to map the layers of a NN on a group of systolic arrays, each composed of several instances of one approximate multiplier. The arrays are part of the same accelerator, with each region processing only one layer of the network. Contrary to [15], the weights are not updated; therefore, the original weights can be used with different approximate configurations. However, considering several static multiplier architectures is not a scalable approach for a general-purpose processor due to the area overhead; this method also impacts flexibility in a custom array accelerator. Our work proposes a single runtime-reconfigurable multiplier with 256 approximation levels, trading off the complexity of additional control logic with increased flexibility. In [17], Tasoulas et al. propose a methodology based on the modification of the bias parameter of each layer to alleviate the approximation error. Similarly to [15], this approach generates a new set of weights for each approximate NN. However, their multiplier features only three runtime adjustable approximation levels. Moreover, the reconfiguration is handled by chaining two bits to each weight stored in memory, increasing the storage requirements and energy associated with data movement. According to [29] and [30], the resilience of a NN model to adversarial attacks depends on the approximate multiplier adopted. Consequently, using different configurations, including an exact one, is suggested to achieve higher error tolerance in various scenarios. MARLIN applied to [30] would remove the constraint of using a single fixed approximate multiplier, enabling error compensation, used in [15], [17] and [20] and this work to

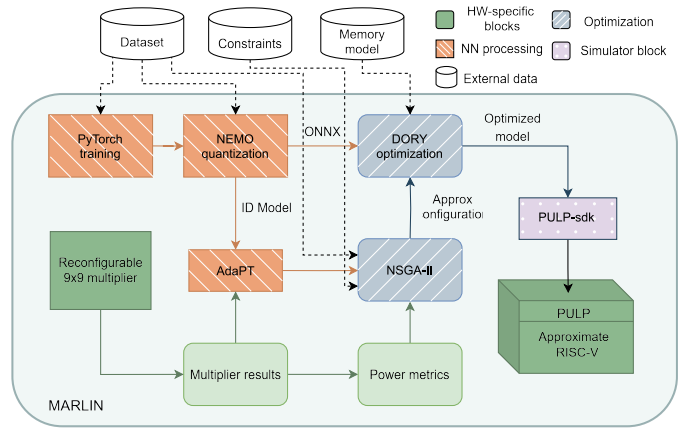


Fig. 2. MARLIN framework with hardware support specific for PULP SoC.

improve the accuracy. Moreover, MARLIN can eliminate the limitations of [29], in which 13 different multipliers are used within each PE to support 13 approximation levels, enabling 21.3 times more approximation levels with a thirteenth of the multipliers instances. Similarly to [18], we selected a RISC-V-based deployment platform, thus simplifying the software configuration of the approximate hardware. Nevertheless, in [18], the configuration signals, handled by a control unit external to the core, are generated by the user, thus relying on his expertise rather than on an automated mechanism. We overcome these limitations by embedding the runtime approximation control inside the instructions processed by the RISC-V core, leveraging the flexibility of the PULP platform.

III. PROPOSED METHODOLOGY

A. Overview

Our framework comprises different building blocks interacting with one another to determine a flow covering from the model definition up to its hardware deployment. From now on, we study the specific case of PULP platform, depicted in Figure 2. The first external input required is a valid dataset, such as MNIST or CIFAR-10, which defines the target task of the NN model. Given a specific application, there are often constraints on the minimum acceptable accuracy or the maximum tolerable energy consumption. Once the training dataset is provided with the specifications, a suitable NN model is identified and described with PyTorch [31]. At this stage, hyperparameters tuning is crucial to obtain consistent results and a model that is already robust to quantization errors. This phase implies choosing the number of training epochs, the type of optimizer, and other learning parameters. A standardized representation of the NN in the form of a data flow graph is required to port the model to PULP. For this reason, the trained NN is passed to NEMO [32], which transforms a floating-point model to an integer one in ONNX format. The precision of the model is fixed at this point in the procedure, with the added constraint that the bit-width of weights and activations cannot be above eight bits, either signed or unsigned. Up to this point of the procedure, the model has no knowledge of the approximation. On the hardware side, a reconfigurable inexact multiplier is designed

and instantiated in MARLIN with a 9×9 bits parallelism. As MARLIN’s optimization software only requires, for each configurable approximation level, a look-up table (LUT) storing all the possible results for each couple of input operands and the average power to execute a single multiplication, the multiplier block is interchangeable. A single runtime reconfigurable approximate unit or several multipliers with fixed approximation levels could be integrated into the framework with little or no modification. Once this high-level description of the computational unit is available, the approximate model can be implemented and tested through the AdaPT library [33]. Any NN topology built with PyTorch’s convolutional and fully connected layers can be easily included in MARLIN by overloading the layer definitions with the AdaPT ones without retraining or changing the model architecture. MARLIN solves the complex multi-objective problem of assigning an optimal approximation level to each layer through NSGA-II, described in Section III-B. It requires repeated simulations of the model with the selected configurations to evaluate their accuracy and power consumption. The obtained Pareto front will show different possible trade-offs between accuracy and power, corresponding to the two fitness functions NSGA-II tries to optimize. The last step that MARLIN performs on the software side is the C code generation to execute the model on the target hardware, presented in Section III-D. A modified version of DORY [34] is used to accomplish this task. This is the first part of MARLIN which requires knowledge of the actual hardware architecture, including a detailed high-level description of every memory level size and latency to perform memory tiling effectively. For this work, PULP was selected as the target platform among those supported. DORY receives as an input the ONNX model generated by NEMO and additional node-by-node dictionary of the NN containing information of the approximation of each layer retrieved by NSGA-II. The modified DORY tool generates the C code for the provided approximate architecture with the received configuration. For this purpose, DORY has to be aware of the modifications the PULP platform undergoes. An approximate unit is added to the execution stage of the cluster cores to approximate all the relevant instructions in the computation of convolutional layers. It is based on the same reconfigurable multiplier, whose LUTs are used by NSGA-II and AdaPT. This unit is managed through a dedicated CSR in charge of activating, deactivating, and configuring its approximation level. In Section III-E is discussed how the modified DORY automatically inserts CSR write and set instructions in the C code of the model to enable the approximate unit when required. The final code runs on the PULP platform through PULP-SDK. The model can be executed by providing input data read from the external L3 memory while the weights are stored in L2 or L3 memory, depending on their sizes. The support of a real hardware RTL on which the model can run is crucial for the validation of the proposed co-design methodology, allowing accurate estimations of the metrics of interest on a complex system.

B. Genetic Search of Optimal Inter-Layer Approximation

In this work, we use NSGA-II, to solve the multi-objective problem of finding NN configurations with different trade-offs

Algorithm 1 Approximation Level Selection With NSGA-II

```

1: ▷  $M$  is the quantized exact model
2: ▷  $axx\_mult$  is the approximate multiplier
3: ▷  $Ng$  is the number of generations
4: ▷  $Np$  is the population size
5: ▷  $Pc$  is the crossover probability
6: ▷  $Pm$  is the mutation probability
7: ▷  $\vartheta$  is the chromosome of  $L$  elements, in range  $[0, A]$ , storing the mult. configuration
8: ▷  $f_1(\vartheta), f_2(\vartheta)$  are the fitness functions to optimize
9: ▷  $P_n$  is the population at iteration  $n$ , with size  $Np$ 
10: ▷ Initialization
11:  $L \leftarrow count(M.Conv)$  ▷ Number of Conv. layers in the model
12:  $A \leftarrow A_0$  ▷ Number of approximation levels for multiplier
13:  $P \leftarrow P_0$  ▷ Initial population vector randomly set
14:  $f(P_0) \leftarrow (f_1(P_0), f_2(P_0))$  ▷ Initial fitness evaluation
15: ▷ Execution
16: for ( $n = 0; n < Ng; n++$ ) do
17:    $Q_n \leftarrow Tournament(P_n, Pc, Pm)$ 
18:    $retrain\_models(M, axx\_mult, Q_n)$ 
19:    $f_1(Q_n) \leftarrow 1/accuracy(M, axx\_mult, Q_n)$ 
20:    $f_2(Q_n) \leftarrow energy(M, axx\_mult, Q_n)$ 
21:    $f \leftarrow (f_1, f_2)$ 
22:    $R_n \leftarrow P_n + Q_n$  ▷ Total population, size  $2Np$ 
23:   for each  $\vartheta$  in  $R_n$  do
24:      $Rank(\vartheta)$ 
25:      $F_i \leftarrow F_i \cup \vartheta$  ▷  $F_i$  are the fronts
26:   end for
27:   for each  $\vartheta$  in  $R_n$  do
28:     for each  $\phi_k$  in  $f$  do
29:        $dis_{\vartheta} \leftarrow dis_{\vartheta} + Crowding\_distance(\vartheta, \phi_k)$ 
30:     end for
31:   end for
32:   Order  $R_n$  based on fronts and crowding distance
33:    $P_{n+1} \leftarrow$  best  $Np$  solutions in  $R_n$  ▷ Update iteration counter
34: end for
35: return  $\vartheta_{best}$  ▷ Optimum Pareto front is returned

```

between energy and accuracy. NSGA-II is a multi-objective genetic algorithm that evolves a population of solutions using non-dominated sorting and crowding distance assignment to classify and rank individuals based on their dominance and diversity. Crossover, i.e., recombination of different chromosomes, and mutation, i.e., variation of a gene, are applied to create offspring solutions, which are then integrated with the parent population. The selection process favors solutions from less crowded Pareto fronts and those with higher crowding distances, promoting the front exploration and providing a diverse set of non-dominated solutions [23]. The motivations for choosing the NSGA-II algorithm are its proven effectiveness in multi-objective optimization and relative ease of implementation and tuning compared to other alternatives such as reinforcement learning or Bayesian optimization. NSGA-II generates a set of optimized approximate NN configurations and selects for each one which approximation level is more suitable for each convolutional layer. Algorithm 1 details the NSGA-II search flow. Each chromosome has a dimension L , which is the number of layers composing the NN. The alleles of each gene are encoded as an integer number between 0 (exact level) and A , which is the number of approximation levels supported by the multiplier. Single-point crossover is used to combine chromosomes while maintaining inter-layer dependencies between approximate configurations, a strategy used in [20] to reduce the effect of computation errors on the NN accuracy without retraining. At the beginning of each iteration, Np approximate NNs are retrained with 10% of the training split (0.1 epoch). Then, the accuracy is evaluated with the validation dataset. Contrary to previous works [15], [17], the accuracy of candidate inexact NNs is not evaluated

immediately, but after a quick retraining with a fraction of an epoch. By leveraging partial retraining and validation, each NN configuration is evaluated by its resilience to computation errors and the retraining effort required to recover from such errors. Solutions with faster recovery will have higher validation accuracy than others that are less fit, using the same number of training samples, and therefore have an evolutionary advantage. Therefore, retraining (or fine-tuning) is used to compensate for the error and enhance the design space exploration. For what concerns the fitness evaluation in Algorithm 1, the inference energy is estimated as in [15] and [17] by multiplying the number of multiplications of each layer of the model M with the average energy of the approximate multiplier when set to the approximation level defined by the corresponding gene of chromosome ϑ . After the evaluation of the two fitness functions, the algorithm continues with the mutation, crossover, tournament selection, ranking, and finally, the evaluation of the crowding distance and the generation of the new front. The cycle starts anew until all the N_g generations have been evaluated.

C. Reconfigurable Approximate Multiplier

In this work, we employ a single-cycle multiplier architecture to introduce minimum modifications in the control flow of the RI5CY core. As our primary purpose is guaranteeing maximum versatility and ensuring portability to different hardware with minimum effort, a parallel multiplier architecture based on the Dadda reduction tree [35] is selected. The Dadda algorithm is employed to compress, through half-adders and full-adders, the matrix of partial products generated in the first step of the multiplication, following an as late as possible approach. It is preferred to the Wallace structure as it shows lower delay and complexity. The modified Baugh-Wooley algorithm [36] is employed to handle signed multiplication with minimum overhead in the size of the partial product matrix. Both techniques are general and scalable to arbitrary operand bit-width. A variation of the truncation mechanism proposed in [37] is identified as the target strategy to manage the dynamic setting of approximation and precision. It allows for easy support of approximate and exact configurations, both for full and reduced bit-width of the operands. Truncation relies on a masking signal to select specific columns of the partial product matrix to fix at zero to reduce the switching activity, hence dynamic power, of the logic gates in that section of the matrix, at the expense of an incorrect output. The number of reconfiguration levels is selected considering that when the approximation is extended to the most significant half of the result, the error becomes unbearable, as argued in [38] and [39]. An externally configurable masking signal noted as a , is introduced to manage the selection of the approximation level, as shown in Figure 3 for the case of 9-bit inputs and a on eight bits. Contrarily to [39], each mask bit a_j of a corresponds to a column of the matrix; there is no sharing of the configuration signals. From bit 2 onward, the probability of the output bit being one or giving a carry-out is higher than 50%, as intuitively proven by the fact that the number of bits stacked in the columns

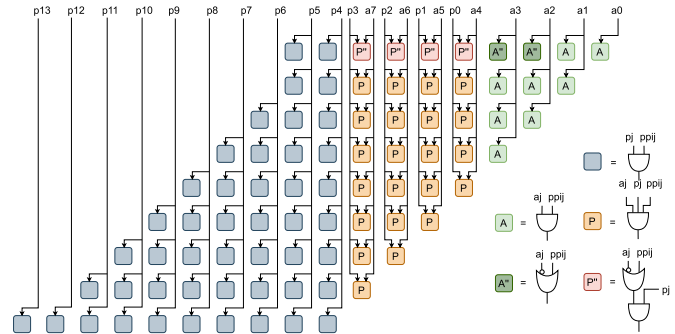


Fig. 3. Precision and approximation configuration management for the proposed multiplier. The approximation level is selected with the mask a , while the precision is selected with the mask p . a_j indicates the j^{th} bit of the `approx_mask` signal a , p_j the j^{th} bit of the `precision_mask` signal p , while pp_{ij} is the j^{th} bit of the i^{th} partial product evaluated according to modified Baugh-Wooley algorithm.

of the matrix is greater than two (Figure 3). This high likelihood justifies the choice to gate the first row of the partial product matrix, from position 2 to 7, to one, when the corresponding bit of the approximation mask is active, and it is implemented through the OR with a_j complemented in Figure 3. All other bits are gated to zero, similarly to [37], using two-inputs AND gates for the masking. An additional feature of the designed architecture, which is uncommon to most approximate multipliers, is the capability of runtime reconfiguration of the precision of the operands. A precision masking signal p is introduced to perform data-gating on the partial product matrix using a mechanism similar to the approximation. The p mask is externally configured according to the precision of the expected result, thus allowing power saving when mixed-precision multiplications are required. The minimum supported bit-width for the input operands is fixed to two. The precision mask has the length of the output minus four. Figure 3 shows the precision signal on fourteen bits p_j covering the most significant part of the partial products. When a precision mask bit is set to zero the corresponding column of the matrix is entirely zeroed. The complete logic inserted in the generation of the partial product matrix to manage multiple approximation and precision levels is depicted in Figure 3.

D. Reconfigurable Approximate RISC-V Core for PULP SoC

The RI5CY core architecture instantiated in the PULP cluster must be adapted to enable reconfigurability in terms of approximation and precision. The first issue to tackle to introduce inexact operators in the core is how to expose them in the instruction set architecture (ISA) so that a programmer can effectively use them. A possible solution is the one proposed in [18]: adding custom instructions that, when decoded, configure the execution stage to use approximate operators. However, this approach requires an additional instruction for each inexact arithmetic operation supported by the hardware, defined with a new custom format capable of encoding the approximation level. Another drawback is related to the fact that, in this specific case, the C executable code is generated automatically by the DORY tool. If custom instructions were used, the user would have to replace the standard instructions

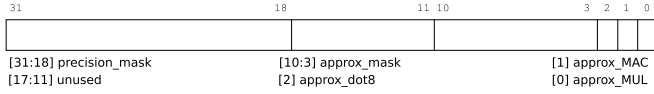


Fig. 4. The approx CSR configuration.

with the custom ones, whenever necessary, analyzing the generated C code line-by-line. The same could be achieved by making the compiler aware of the approximated instructions and where they are needed, but that would be time-consuming to implement and maintain. The methodology suggested in this work addresses flexibility and simplicity by defining a new custom CSR handling all the control and configuration of approximate operators. This approach is scalable; a single 32-bit register can manage all the new operations and does not occupy additional instruction encoding space. It also enables reconfiguration, as part of the register bits control the approximation and precision level. Finally, it is much more programmer-friendly as it does not require significant changes in the C code of the microcontroller, except for the addition of CSR instructions. In order to achieve these results, the proposed methodology to enable the online configuration of the approximate multiplier relies on the following steps. First, a CSR write instruction sets the `precision_mask` and `approx_mask` fields according to the specification of the layer. Secondly, before the computation starts, a CSR set instruction enables `approx_mac` and `approx_dot8`, which are disabled when the computation is over. Each CSR instruction takes one clock cycle. In the general case, the last couple of CSR instructions are executed a number of times which depends on the tiler split performed by DORY. Their position in the code is optimized to produce minimum overhead in the control flow, considering the presence of MAC instructions that must produce the correct result. The usage of three instructions, rather than two, is forced by the specific organization of the template C files provided by DORY and PULP-NN C library [22]. The CSR instruction activating the approximate unit is the one executed more frequently. It is located before the `matmul` function, whose pseudocode and number of assembly instructions are depicted in Algorithm 2. In a pessimistic estimation, a CSR set is performed once for each `matmult` function call, providing a quantitative measure of the reconfiguration overhead on the execution time. The GCC compiler is extended to account for the new `approx` CSR, whose fields are given in Figure 4.

The Xpulp ISA extension [22] provides additional multiply-related instructions compared to the basic ones of RV32M. Some of these, such as MAC and SIMD dot products, are useful for NN inference. Here, the choice is to provide an approximate implementation only for instructions used in convolutional and linear layers. An in-depth analysis of the disassembly code produced by custom convolutions and a complete NN is performed to select them. The assembly instructions included in these benchmarks are approximated, together with others for which it is straightforward to extend support; they are all listed in Table I. In this first implementation, the approximate pipeline only computes 8-bit multiplications, even when the issued instruction expects a 32-bit or 16-bit operation.

Algorithm 2 PULP-NN `matmul` function pseudocode

```

1: ▷ ch_in/ch_out input/output channels of the Conv layer
2: ▷ k_x/k_y filter dimension along x/y
3: ▷ im2col is ch_in · k_x · k_y
4: ▷ col_cnt_im2col is im2col & 0x3
5: ▷ chan_left is ch_out & 0x3
6: ▷ Initialization
7: Load params. from stack and define variables ▷ 26 instr
8: ▷ Execution
9: for (i = 0; i < ch_out >> 2; i ++) do
10: Setup ▷ if first iteration 41 instr, else 6 instr
11: for (j = 0; j < im2col >> 2; j ++) do
12: Setup ▷ 15 instr
13: Multiply and accumulate + save ▷ 15 instr · (im2col >> 2) + 9 instr
14: end for
15: if (im2col >> 2 == 0) then; Setup end if ▷ 12 instr
16: while (col_cnt_im2col != 0) do
17: Setup ▷ 4 instr
18: Multiply and accumulate + save ▷ 15 instr · (im2col >> 2) + 2 instr
19: end while
20: Quantize and save results ▷ 54 instr
21: end for
22: Setup ▷ 10 instr
23: while (chan_left) do
24: Setup ▷ if first iteration 23 instr, else 1 instr
25: for (j = 0; j < im2col >> 2; j ++) do
26: Setup ▷ 6 instr
27: Multiply and accumulate + save ▷ 6 instr · (im2col >> 2) + 4 instr
28: end for
29: if (im2col >> 2 == 0) then; Setup end if ▷ 6 instr
30: while (col_cnt_im2col != 0) do
31: Setup ▷ 4 instr
32: Multiply and accumulate + save ▷ 6 instr · (im2col >> 2) + 1 instr
33: end while
34: Quantize and save results ▷ 13 instr
35: end while
36: Save parameters and return ▷ 24 instr

```

TABLE I
APPROXIMATE INSTRUCTIONS MNEMONICS

MAC	MUL		DOT8	
p.mac	mul	p.mulsN	pv.dotup.b	pv.sdotup.b
p.macsN	p.muls	p.muluN	pv.dotusp.b	pv.sdotusp.b
p.macuN	p.mulu		pv.dotsp.b	pv.sdotsp.b

This restriction cannot cause any error assuming that NN layers quantization is always on 8 bits or below, which is the ordinary case. The instructions for which approximate support is provided are split into three subgroups, according to Table I. For each category, the `approx` CSR has a configuration bit; when this bit is set, all the instructions belonging to that group are executed in approximate mode. Besides the custom CSR, a unit responsible for inexact computation is inserted in the execution stage of the pipeline alongside the exact multiplier unit, as shown in the high-level block diagram of the approximate core in Figure 5.

This design choice requires some modifications in the decoding phase of the instruction. Based on some control signals, the decoder has to activate either the correct or the inexact unit. The arithmetic block that is not selected for the instruction currently in the decode stage does not perform any operation in the next clock cycle as its inputs are not updated. Four instances of the designed multiplier are allocated in the reconfigurable approximate unit, as in Figure 6. They are all used in parallel to perform SIMD dot products on 8 bits, while only one is activated for MUL and MAC-related operations.

E. Approximation in PULP Toolchain

Part of the PULP toolchain must be adapted to enable run-time approximation. Through NEMO and DORY libraries, the

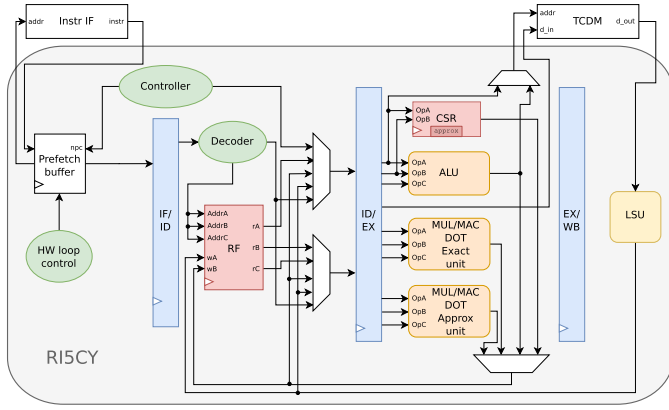


Fig. 5. RISCY pipeline with approximate operations support.

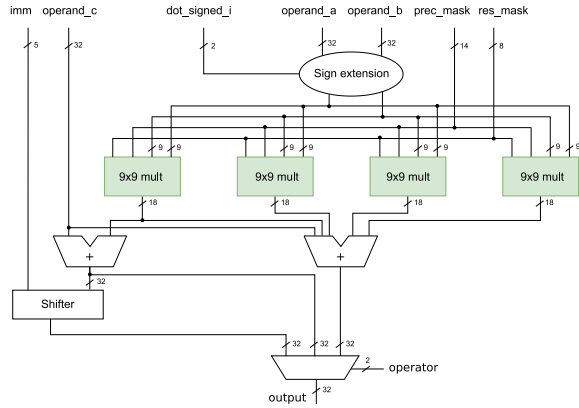


Fig. 6. RISCY approximate multiplier unit. The leftmost multiplier is in charge of MUL and MAC-related operations. The shifter is for immediate instructions with the N suffix in Table I. All multipliers work in parallel to execute dot8 operations and their result is fed to a 32-bit five-operands adder. The sign extension block handles the split of the 32-bit operands into four 8-bit chunks and their sign extension according to the decoded instruction.

PULP platform offers software support to generate executable C code tailored to its architecture, starting from a PyTorch NN model. NEMO is a PyTorch complementary framework developed as a support tool to transform an already trained, full-precision NN into an integer one, performing the quantization and calibration of the model. DORY is an open-source tool for optimizing NNs mapping on PULP and other MCUs. Two building blocks of DORY, the configurable templates and PULP-NN back-end functions, are modified to automatically add the approximate CSR instructions in proper points of the C code, while the mapping optimization is unaffected. Besides an ONNX graph, the modified DORY uses as input a JSON file containing a layer-by-layer description of the quantization and approximation of the NN. Once these parameters become part of the DORY intermediate representation, they are used to fill hardware-specific template files with the correct CSR setting and generate the C code for the different layers. Relying on a JSON dictionary guarantees flexibility, as new items can be defined for each node in the network. Furthermore, it is general; at this level, every type of approximate multiplier could be available, either reconfigurable or not. Moreover, as the precision information on the layer is kept separate from the approximation level, it is possible to configure the layer as

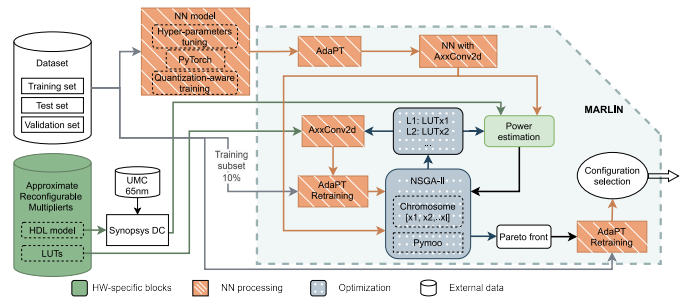


Fig. 7. MARLIN framework and computing setup for software simulation.

exact but with reduced precision. This choice allows to save power by leveraging operations with reduced bit-width rather than with inexact computation.

IV. EXPERIMENTAL RESULTS

This section presents the computing setup used to conduct experiments to validate the proposed methodology, summarized in Figure 7. We synthesized and tested the modified RISCY with the reconfigurable multiplier and extracted relevant hardware metrics of the core and the arithmetic operator alone. Additionally, we compare our approach against state-of-the-art techniques that apply layer-wise approximation.

A. Multiplier Characterization

A 9-bit reconfigurable multiplier is designed according to the methodology in Section III-C to compute SIMD 8-bit dot products supporting all possible combinations of signed and unsigned operands in RISCY core. The multiplier is synthesized with Synopsys Design Compiler (DC) using the UMC 65 nm process technology library. The design is wrapped by a group of input and output registers to ease the enforcement of timing constraints. Similarly to [38], the target clock period is set to 2 ns, making the multiplier critical path delay compatible with the one it shows on the synthesized core. The `compile_ultra` command is issued to generate the gate-level netlist. Post-synthesis simulation is performed on 100000 random input samples to back-annotate the switching activity for accurate power estimation, as in [40]. Random input samples are a common approach in literature to characterize the power profile of approximate multipliers, [28], [37]. Table II shows the main hardware metrics and mean-relative error distance (MRED) obtained for the maximum precision configuration with different approximation levels.

$$MRED = \frac{1}{n} \sum_{i=1}^n \frac{|\hat{y}_i - y_i|}{|y_i|} \quad (1)$$

The MRED, a commonly used metric to estimate the performance of inexact arithmetic units [38], [39], [40], is defined in Equation (1), where n is the number of possible combinations of input values (i.e. $n = 2^{18}$, for a 9×9 multiplier), and \hat{y}_i and y_i are the i^{th} approximate and exact results, respectively. Error metrics are evaluated through exhaustive simulation on the entire inputs dynamic [38], [40]. Table II presents the same estimations, obtained with the same constraints and testing

TABLE II

METRICS OF THE 9×9 SIGNED RECONFIGURABLE MULTIPLIER AND COMPARISON WITH AN EXACT 9×9 MULTIPLIER

Design	Area [μm^2] (GE) ¹	Arrival time [ns]	Approx level	Total power [μW]	MRED
Exact	607.3 (422)	1.7	-	414.0	0
MARLIN	822.6 (572)	1.8	0	241.2	0
			127	183.0	0.07
			255	164.4	0.18

¹GE is the 2-input drive-strength-one NAND gate equivalent area.

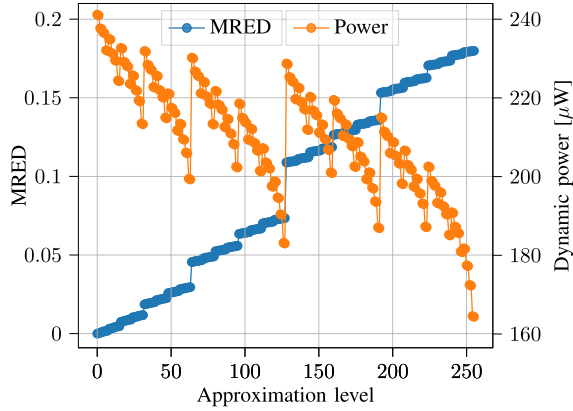


Fig. 8. MRED and dynamic power variation of the proposed multiplier with the approximation level for the full-precision 9-bit inputs configuration. The approximation level on the x-axis corresponds to the 1's complement of the `approx_mask` value.

conditions, for an exact 9×9 signed multiplier described behaviorally in HDL and optimized by Synopsys DC, through Synopsys DesignWare (DW) library. Our multiplier has an area overhead of 28%, due to the additional logic for online reconfigurability. This feature does not impact on the critical path, as it remains under the 2 ns constraint. Finally, our multiplier, in the exact configuration, saves 41.4% of power compared to the one by Synopsys DW, while the highest approximate level saves up to 60.1%.

Although the dynamic power variation with the approximation setting does not follow a monotonic trend, as can be observed in Figure 8, sub-optimal configurations are retained as they come at no hardware cost in area, power and latency once the 8-bit `approx_mask` signal is inserted in the multiplier logic. Every level has its error distribution, which can be optimal for a specific NN layer. An optimal subset of the 256 configurations might be selected offline depending on the dataset and NN analysed. However, the proposed methodology aims to be application-agnostic and versatile to several use-cases, thus hardware and software provide support for the most generic scenario. The jumps in power and MRED in Figure 8 can be explained by looking at the logic in Figure 3. The MRED shows higher steps when the approximation moves towards columns on the left (e.g., from configuration 63 to 64, or from 191 to 192). On the contrary, more power is saved when more columns, as far to the left as possible, are gated, reducing the switching activity of the compressors in the Dadda Tree. This condition in Figure 8 corresponds to `approx_mask` values $\bar{a} = 2^j - 1$, $j \in [0, 1, 2, 3, 4, 5, 6, 7, 8]$. Consequently, when `approx_mask` is set as above, that configuration will save more power than

TABLE III

COMPARISON BETWEEN THE MARLIN 8×8 SIGNED MULTIPLIER AND STATE-OF-THE-ART APPROXIMATE MULTIPLIERS

Multiplier	Conf	Exact conf	Online reconf	MRE	Area [μm^2] (GE)	Dynamic power [μW]
Ha [41]	-	✗	✗	0.102	461.2 (321)	170
Strollo [40]	-	✗	✗	0.053	496.8 (345)	181.6
Yang [42]	1	✗	✗	0.031	529.2 (368)	222.3
	2	✗	✗	0.041	516.2 (359)	206.6
	3	✗	✗	0.069	500 (348)	190.9
Mul8s [28]	1KV6	✓	✗	0	541.1 (376)	167.6
	1KX5	✗	✗	0.089	378 (263)	116.3
	1L2N	✗	✗	0.274	200.9 (140)	60.9
	1L12	✗	✗	1.347	126 (88)	36.6
de La Guia [37]	0	✓	✓	0	650.9 (452)	188.3
	127	✓	✓	0.374	650.9 (452)	130.3
	255	✓	✓	1.065	650.9 (452)	109.5
MARLIN	0	✓	✓	0	652.7 (454)	188.6
	127	✓	✓	0.236	652.7 (454)	130.6
	255	✓	✓	0.621	652.7 (454)	109.9

the subsequent ones. Furthermore, it is a Pareto optimal point since all the successive configurations imply the next columns to the left to be approximated, thus increasing the MRED.

Table III compares different state-of-the-art techniques to design approximate multipliers. All multipliers are 8-bit signed and have been synthesized with a clock period of 2 ns and characterized as for the 9×9 case. For a fair comparison, our multiplier is rescaled on 8 bits. The design choice to fix some bits of the partial product matrix at one rather than zero when the corresponding columns are approximated improves the MRED by up to 41.7% compared to [37] truncation approach, with negligible area and power overhead. Compared to [40], [41], and [42], all based on approximate 4-2 compressors, our multiplier has lower power consumption, for corresponding MRED, while still covering a much wider error dynamic. Furthermore, the approximate compressors approach, even when runtime error tuning is implemented [38], [39], cannot provide an exact configuration. This implies the need to pair an exact multiplier with the approximate one to manage operations, such as control flow ones, which must produce the correct output, unacceptably increasing the total area. This consideration still holds for Evoapproxlib multipliers [28]. Although, according to Table III, [28] show better area and power metrics compared to ours, the absence of reconfigurability precludes their compatibility with MARLIN. As in [15], the implementation of layer-wise approximation with [28] requires to instantiate as many multipliers as the number of approximation levels, which becomes inconceivable above certain values due to control, area, and power overhead. In conclusion, our multiplier offers several power-error trade-offs, spanning the MRED dynamic of most of the 8×8 multipliers compared in Table III, standing as the cheapest and most flexible solution to implement layer-wise approximation. Our multiplier, unlike [28], [38], [40], [41], [42], also enables runtime selection of the result bit-width to add versatility and reduce power when full precision is not required. For the 9-bit architecture, output precision from 18 bits down to 4 bits is supported through data-gating on the most significant columns of the Dadda tree, with a maximum power saving of around 62%. In Table IV, we evaluate the trade-off of runtime precision setting with a ResNet-20 model executed with and without data-gating, and with different bit-widths. The average

TABLE IV

RESNET-20 MULTIPLIER POWER WITH AND WITHOUT DATA-GATING

Activations precision	Weights precision	Avg mult pow full precision	Avg mult pow reconfigured	Absolute accuracy	Relative accuracy
8	8	239.15 μ W	237.93 μ W	91.50%	100%
6	4	227.85 μ W	170.09 μ W	91.43%	99.92%
4	4	225.85 μ W	125.35 μ W	89.87%	98.22%

TABLE V

PERFORMANCE AND AREA COMPARISON FOR EXACT AND APPROXIMATE RI5CY AND THEIR RELATIVE MULTIPLIER UNITS

		Exact RI5CY	Approx RI5CY
Area [μ m ²] (GE)	Exact mult	14842.8 (10k)	
	Approx mult	-	4737.2 (3k)
	Total	60621.1 (42k)	67006.8 (47k)
Timing [ns]	Exact mult	4.45	
	Approx mult	-	4.41

full precision power is evaluated with the multiplier configured to execute 9×9 bit multiplications, although input operands are quantized to lower precision. The average reconfigured power is evaluated when the masking signal p is set to match the input operand precision.

B. Approximate RISC-V Core Characterization

The RI5CY core featuring the approximate extension is synthesized to extract area, delay, and power estimations using Synopsys DC and the UMC 65 nm library. The clock period is set to 5 ns. The timing constraints were relaxed with respect to the ones for the multiplier alone to also accommodate in the cycle time the four-operand 32-bit adder that follows it, as can be observed in Figure 6. As a matter of fact, the approximate multiplier instance in the core has a delay of around 1.9 ns, which makes its implementation mapping and, therefore, its energy contribution consistent with the analysis previously performed with a 2.0 ns clock period. The two cores with exact and reconfigurable approximate operators are both synthesized using the command: `compile_ultra -no_autoungroup -no_boundary_optimization -timing -gate_clock`. Table V compares area and timing values obtained. The delay constraints are satisfied by both designs, and from the fourth column of Table V it can be observed that our multiplier does not interfere with the microprocessor critical path which remains in the exact multiplier unit. The area overhead caused by the approximate unit alone is 7.8%, while the total overhead, considering the additional control part and the approx CSR, is 10.5%. The extra area cost is mainly due to the allocation of four reconfigurable multipliers in order to manage 8-bit dot products. We consider this overhead acceptable as this is the first prototype of this architecture; however, it could be significantly decreased if our four multipliers replaced the exact ones, which is possible since they also feature a non-approximate mode.

The RTL model of the RI5CY is replaced by the gate-level netlist for all cores in the PULP cluster to enable post-synthesis simulation and power estimation on a demonstrative use-case. A simple NN model is designed with PyTorch and used as a benchmark on MNIST dataset to verify the correct behavior of

TABLE VI

CUSTOM NN ARCHITECTURE DESCRIPTION

Layer name	Output size	Kernel size	Output channels	# Mult
conv1	28x28	7x7	3	115224
conv2	28x28	5x5	8	470400
max pool	14x14	3x3	8	0
conv3	14x14	3x3	10	141120
conv4	14x14	3x3	16	282240
max pool	7x7	3x3	16	0
conv5	7x7	3x3	24	169344
max pool	3x3	3x3	24	0
linear	1x10	9x24	1	2160

TABLE VII

POWER CONSUMPTION AND ENERGY SAVING OF THE MULTIPLYING UNIT WITH DIFFERENT LAYER-WISE CONFIGURATIONS FOR THE TARGET NN

Configuration	Test Acc [%]	Average RI5CY mult power [μ W]	Relative RI5CY mult energy saving	Relative NSGA-II energy saving
Exact	98.7	10.46	0%	0%
[0, 0, 0, 0, 0]	98.7	2.606	75%	42%
[59, 31, 15, 12, 3]	98.7	2.509	76%	46%
[59, 31, 15, 31, 31]	98.5	2.474	76%	48%
[255, 63, 15, 31, 11]	97.8	2.412	77%	50%
[255, 126, 3, 63, 63]	91.3	2.403	77%	53%

the entire framework and to collect power metrics. It comprises five convolutional layers, each followed by a ReLU activation function, and a final linear layer. The entire structure is depicted in Table VI. The model is trained for 30 epochs, with a batch size of 32, an initial learning rate of $3 \cdot 10^{-3}$, with a step factor of 0.3 every 5 epochs. Stochastic gradient descent with momentum 0.9 is used with a weight decay of 10^{-3} . The designed NN is run on the PULP platform for a single input image. For this model, the overhead of the CSR instructions execution can be quantified, according to Algorithm 2, in the worst case, which is the first convolutional layer, as one CSR set instruction every 403 instruction (0.25%). In the best case, which is the last convolution, the extra cost is 0.026%. This results in a negligible performance overhead due to the CSR switching, and thus of reconfiguration, on the overall processing. Through Siemens QuestaSim, the VCD dumps of the entire core and the approximate and exact multiplying units are collected. They are used as inputs for Synopsys Power Shell to extract power metrics based on the actual switching activity. Simulations are performed using the multipliers configurations obtained from the NSGA-II run that achieve accuracy over 90% with no retraining. For every configuration, an example for each of the ten possible categories is fed to the network, meaning numbers from zero to nine for MNIST. The exact post-synthesis RI5CY core is simulated with the same inputs, and the power of the accurate multiplier unit is collected; all results are averaged. Table VII reports, for the configurations listed in the first column, the NN test accuracy and, in the third column, the power of the multiplier unit (the exact one for the exact configuration in the first row, the approximate one for all other cases) averaged over the ten simulations. The fourth column contains the relative energy saving of the multiplier unit measured post-synthesis, the last column shows the relative energy saving estimated at the end of the NSGA-II search, as described in Section III-B. The first row of Table VII

contains the power estimation of the exact RI5CY multiplier unit, where all operators, including the multipliers computing dot8 instructions, are described behaviorally, thus leaving the architecture selection to Synopsys DW. Consequently, for a meaningful comparison, the reference model for the NSGA-II relative estimation is the average energy consumed by a behavioral 9-bit multiplier synthesized by Synopsys DC, with the same settings of the approximate multiplier. Although the exact multiplier always executes housekeeping operations, these are a negligible fraction of its overall workload when all NN multiplications are mapped on it; thus, their contribution to the average power is minimal. Therefore, since the number of multiplications of the NN model is fixed, and so is the time the multiplier stays active, the relative energy is considered equivalent to the ratio between the average power of the approximate unit in the modified RI5CY and that of the exact one in the unmodified core.

The fourth column of Table VII shows that the obtained average energy saving on the multiplier unit is at least 75% when comparing the exact core and the approximate one with all multipliers configured as accurate (first and second row in Table VII). The maximum saving is 77%, which is more than 20% higher than the high-level estimation performed in NSGA-II. However, the advantage of adopting different approximate configurations is heavily reduced compared to the initial evaluation. This can be observed by rescaling the energy results in the fourth and fifth columns of Table VII with respect to the exact configuration of our multiplier. The highest estimated energy reduction, with respect to the model using the exact configuration of our multiplier for all layers, is 7.7%, with an accuracy loss of 7.4%, while the predicted saving was 20.1%. The cause of the gain drop, obtained by configuring the multiplier with a higher approximation, has to be addressed to the chosen task for the network. When the average power of the multiplier is estimated, 100000 random values with uniform distribution are used as inputs to the multiplier. However, the MNIST dataset is composed of black numbers on a vast white background, which means that the network inputs and, consequently, those of the multipliers are not uniformly distributed. Both input images and intermediate activations show a high concentration of zeros, contrary to the initial assumption. The main consequence of most values being zero is that data-gating, which is the primary source of power saving when approximation is applied, becomes ineffective as the operands are already zeros and have a low switching probability themselves. A higher sensitivity of our multiplier to zero input operands, compared to the DW one, could also explain the increased relative energy saving in the example with respect to the estimates used during the NSGA-II search. Even acknowledging the difference in the statistics of the operands, we run the optimization algorithm using the estimated average energy computed with uniformly distributed inputs, keeping it data-agnostic, as commonly done in state-of-the-art optimization frameworks, where performance metrics are estimated independently from the statistics of the dataset [3], [10], [11], [12]. The latter enables our search algorithm to generalize to new data and thus demonstrate the efficacy of our method, an approach that was also used in

TABLE VIII
NEURAL NETWORKS USED IN THE EXPERIMENTS

Neural network	# Conv. layers	# Mult.	FP32 accuracy	INT8 accuracy	Design space size
ResNet-8	7	12.2M	85.33%	85.43%	$72 \cdot 10^{15}$
ResNet-14	13	26.4M	90.17%	90.32%	$20 \cdot 10^{30}$
ResNet-20	19	40.6M	91.77%	91.50%	$57 \cdot 10^{44}$
ResNet-32	31	68.9M	92.65%	92.58%	$45 \cdot 10^{74}$
ResNet-50	49	111.3M	92.88%	92.60%	$10 \cdot 10^{117}$
ResNet-56	55	125.5M	93.14%	93.11%	$28 \cdot 10^{131}$

[15], [16], [17], and [24] to estimate the energy reduction with approximate multipliers.

C. Benchmark With CIFAR-10

We used 6 variations of the ResNet model architecture [43] to experiment with shallow and deep NNs for image classification, testing the effectiveness of MARLIN with CIFAR-10 [44], a more challenging dataset than MNIST. We based the implementation of our ResNet models on the original paper and used the same model architecture and hyper-parameters, with 44k iterations instead of 64k, substituting the original multi-step scheduling of the learning rate with a cyclical scheduler [45], ranging between 10^{-1} and 10^{-4} . We opted for a cyclical learning rate instead of a stationary one to achieve faster convergence with fewer training iterations during the genetic search. We carried out separate quantization-aware and full precision training for the INT8 and FP32 models. All the experiments with approximate multipliers use the INT8 quantized models; the FP32 results are presented only to provide a comparison with full precision. We used scale quantization with the straight-through-estimator for the weights [13], while the activations are quantized using PACT [46]. Table VIII reports the NNs used in the experiments.

The INT8 accuracy results are evaluated using the approximation level 0 of the proposed multiplier, which provides exact results, for all the layers of each network. The multiplications reported in Table VIII are evaluated for the inference of one $32 \times 32 \times 3$ input image from the CIFAR-10 dataset. The design space size reported in the rightmost column is evaluated as the number of unique approximate layer-wise configurations, evaluated as A_x^L , with A_x being the number of approximation levels of the reconfigurable multiplier, in our case 256, and L the number of layers that can be approximated.

For ResNet-8, ResNet-14, and ResNet-20, we ran the genetic search for 80 generations with a population of 70 individuals, whereas for ResNet-32, ResNet-50, and ResNet-56, we increased the generations to 120. We set both the mutation probability P_m and the crossover probability P_c to 0.8. During the search phase, every approximate NN is retrained with 10% of the training set and the accuracy is evaluated with the validation set (5000 unseen images from the training set). We did not use the test set during the search phase as it would have biased the results and negatively affected the genetic algorithm. In this phase, the NN accuracy influences the evolution of each individual's configuration, i.e., the layer-wise approximation; therefore, to obtain NN models that can

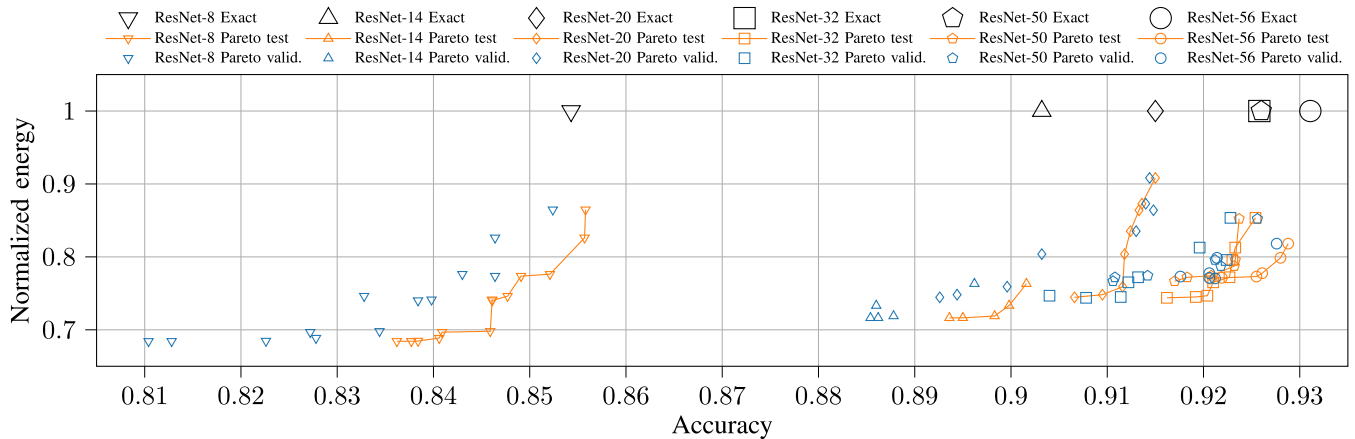


Fig. 9. Top 1% accuracy and normalized energy variation with different ResNet configurations. The *Pareto valid*. blue marks represent the validation accuracy evaluated during the genetic search, whereas the *Pareto test* orange marks represent the corresponding approximate configuration tested after the final retraining.

generalize on new unseen data and prove the effectiveness of our methodology, we removed any correlation with the final test results. Finally, once the Pareto front has been computed, the approximate NNs are retrained for one full epoch and evaluated using the test set.

The accuracy and energy results of only the dominant solution after the full retraining of the Pareto front are reported in Figure 9, providing a visual representation of the energy-accuracy trade-offs our methodology offers. For every NN under test, the absolute accuracy difference between *Pareto valid*. and *Pareto test* marks of each configuration is usually smaller than 1.5%, with even smaller values for deeper models. Therefore, the validation accuracy could represent a good approximation of the final results, justifying the choice of using it in the proposed search strategy. Figure 10 depicts the utilization of approximation levels for each NN layer. It is possible to notice the presence of peaks around levels with an index equal to or smaller than $2^j - 1$, $j \in [0, 1, 2, 3, 4, 5, 6, 7, 8]$, corresponding to the Pareto optimal points of Figure 8. In Figure 10, it is shown how the majority of approximation levels are used in the Pareto front, justifying the choice to maintain power and MRED-dominated configurations as the most efficient levels might not be optimal ones to achieve a high task accuracy. Moreover, when concatenated appropriately, some approximation levels, even the Pareto-dominated ones, might mitigate the effect of computation errors on the final results, a strategy used in [20] to reduce the accuracy degradation. However, Figure 10 also highlights that some approximation levels are never used in this use case. Future development should add the possibility of pruning the search space removing unused solutions or those with the lowest utilization. In these experiments, to prove that our methodology is effective with an ample search space, low- and zero-usage solutions are deliberately kept to test the search algorithm in a worst-case scenario with the highest complexity.

Table IX compares our approach with ALWANN [15] to understand how MARLIN stands against the state-of-the-art. To make a fair comparison, we compare approximate NNs with weights updated after a single epoch retraining for MARLIN and weight fine-tuning for ALWANN. Our method can

TABLE IX
COMPARISON WITH ALWANN [15] WITH 0.5% AND 1% RELATIVE ACCURACY DEGRADATION

Neural network	This work			ALWANN		
	Absolute accuracy	Relative accuracy	Energy	Absolute accuracy	Relative accuracy	Energy
ResNet-8 0.5%	85.21%	99.74%	77.62%	83.16%	99.88%	84.31%
ResNet-8 1%	84.59%	99.02%	69.80%	Same solutions as ResNet-8 0.5%		
ResNet-14 0.5%	89.98%	99.63%	73.32%	85.42%	99.85%	74.34%
ResNet-14 1%	89.50%	99.09%	71.64%	84.77%	99.09%	70.85%
ResNet-50 0.5%	92.14%	99.50%	80.67%	89.08%	99.92%	78.47 %
ResNet-50 1%	91.70%	99.03%	76.67%	88.58%	99.36%	70.02 %

achieve better results for shallower NNs such as ResNet-8 and maintain the same relative gains for ResNet-14, whereas it was not able to achieve higher energy efficiency than ALWANN for ResNet-50. Comparing the absolute accuracy of the NN models, the approximate ResNet-14 within 1% relative accuracy degradation outperforms all the ResNet-50 models presented by ALWANN in top-1 accuracy and, by extension, in energy efficiency, as ResNet-14 has 76.3% fewer multiplications than ResNet-50. Our methodology is competitive, considering that the multipliers used in ALWANN have better area and power-MRED metrics, but are not reconfigurable [15], [28]. The main advantage of a reconfigurable multiplier against several arrays of fixed multipliers is that it is possible to improve the energy efficiency of arithmetic operations with lower area. This approach extended to a systolic array, would require a single array with the same multiplier architecture, whereas ALWANN requires N separate sub-arrays in order to support N approximation levels.

Table X compares MARLIN with the results presented in [17], without including absolute accuracy metrics, as they are not reported. We consider approximate NNs with one-epoch retraining for MARLIN, and approximate NNs with weight fine-tuning with and without additional bias for [17]. Compared to the NNs with no additional bias, the approximate NNs configurations found with MARLIN require up to 13.1% less energy for ResNet-20, up to 13% less energy for ResNet-32, and up to 15.1% for ResNet-56. When an additional error correction bias is added to the convolutional layer in [17], MARLIN can still achieve up to 9.8% less energy

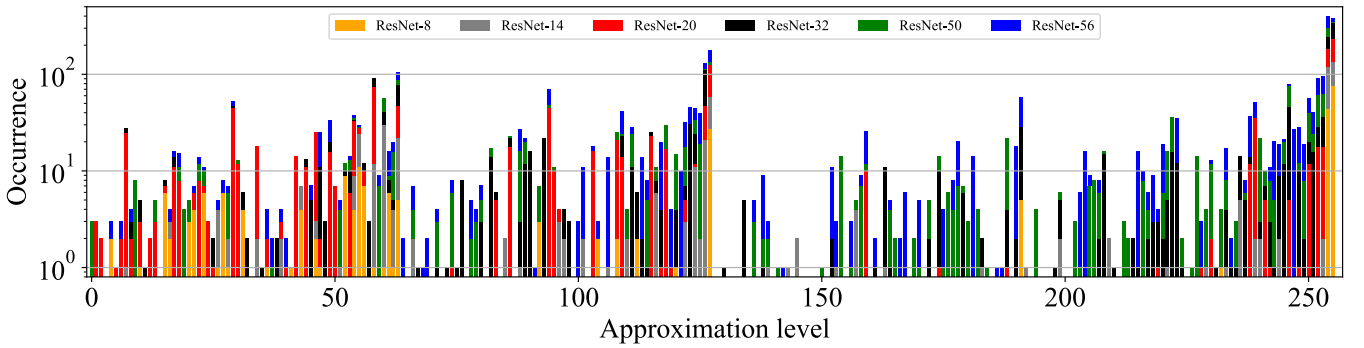


Fig. 10. Approximation levels utilization for all the configurations found for each ResNet model.

TABLE X

NORMALIZED ENERGY COMPARISON WITH [17] WITH 0.5%, 1%, AND 2% ACCURACY DEGRADATION

Neural network	Normalized energy		
	Ours	[17] w/o bias	[17] with bias
ResNet-20 0.5%	75.91%	86.1%	83.1%
ResNet-20 1%	74.46%	85.6%	83.0%
ResNet-20 2%	74.46%	85.1%	82.5%
ResNet-32 0.5%	77.21%	85.7%	81.7%
ResNet-32 1%	74.50%	85.7%	81.7%
ResNet-32 2%	74.39%	85.5%	81.4%
ResNet-56 0.5%	79.87%	94.0%	83.0%
ResNet-56 1%	77.12%	86.1%	83.0%
ResNet-56 2%	77.04%	86.1%	83.0%

for ResNet-20, 8.6% for ResNet-32, and 7.3% for ResNet-56, without increasing the number of parameters and operations. Using more approximation levels proved to be an effective way to further reduce the inference energy, as we had 256 configurations against the 3 used in [17]. We justify these results with the traditional weight-update strategy used in this work and the presence of more approximate configurations. Retraining each configuration is slower and more computationally expensive than the multiplier-specific fine-tuning of [17], but allows a better adjustment of the NN parameters to compensate the computation errors, resulting in higher accuracy.

D. Compatibility With Other Accelerator Architectures

Two important modifications are necessary to port MARLIN to other platforms: adapting the hardware architecture and the mapper to include the multiplier and the configuration instructions. The former would require an additional 8-bit control signal from the PE control unit to set the approximation level. The elongated critical path delay due to the approximation logic could be a problem for some accelerators, but it is not for [8] and [9], which have a critical path compatible with the proposed multiplier. For what concerns the mapper, recalling the discussion of Section II-A, a modification similar to what has been done in Section III-E can be implemented, inserting custom instructions to configure the multiplier, with negligible impact on the execution time. Since the scheduling does not change, the number of computation cycles would also be unaffected. Table XI reports the area and the energy overheads of including and controlling the approximate multipliers in three accelerators, mapping the 19 convolutional layers of the

TABLE XI

MARLIN'S AREA AND COMMUNICATION OVERHEAD APPLIED TO OTHER HW ACCELERATORS

	Eyeriss [9]	DianNao [7]	Simba [8]
# PEs	256	256	1024
PE conf. comm. energy [pJ] (relative)	2138 0.001%	1997 0.001%	2369 0.002%
Mult. area exact [μm^2] (GE)	155468 (108k)	155468 (108k)	621875 (432k)
Mult. area approx. [μm^2] (GE) (relative)	210585 (146k) (+35%)	210585 (146k) (+35%)	842342 (586k) (+35%)

ResNet-20 with 1% accuracy degradation and 74.46% energy of Table X. We used the power model in Timeloop [10] to evaluate the energy used to communicate to the PEs the approximation level of each layer, assuming one off-chip transfer to on-chip memory transfer, and then #PEs transfers from the on-chip memory to the PEs' registers. The configuration energy of the entire NN is always below 0.002% of the total energy evaluated with Timeloop. The area overhead of 35% against exact multipliers can be negligible, considering that they account for less than 10% of the PE area in [8] and [9].

E. Discussion

The optimization approach of Section III-B allowed MARLIN to outperform previous works that relied on parameter fine-tuning [15], [17], leveraging partial retraining. MARLIN was run on a 32-thread Ryzen 5950X CPU with 64GB DDR4 RAM and an Nvidia Quadro RTX A5000. The GPU was used only during the initial training of the FP32 and exact INT8 NNs presented in Table VIII, while the CPU was used to simulate the approximate convolutional layers, as AdaPT only supports CPU computation [33]. The number of threads used during the computation was set to 16 for every experiment to compare how MARLIN execution time scales with different NNs depths. Table XII reports the execution time for the search phase and the training of the last Pareto front of Figure 9. On average, partial retraining is $\approx 6\times$ faster than full retraining. An alternative implementation that leverages the GPU processing power, based on [47], is in development, with the objective of reducing the search time with more complex NN models, allowing for a broader search space analysis. Compared to [15], the iteration time during the search phase is reduced by 72.8% for ResNet-8, 92.3% for ResNet-14, and 85.4% for ResNet-50. This speed-up is due to the increased

TABLE XII
MARLIN'S AVERAGE EXECUTION TIME WITH 16 THREADS

Neural network	Search phase		Final training	
	One iter.	Total	One iter.	Total
ResNet-8	6.8 sec.	10.6 hours	40.9 sec.	24.6 min.
ResNet-14	7.7 sec.	12 hours	79.4 sec.	35.7 min.
ResNet-20	19.6 sec.	30.5 hours	115.7 sec.	90.6 min.
ResNet-32	30.3 sec.	70.7 hours	189.0 sec.	81.9 min.
ResNet-50	47.1 sec.	109.9 hours	296.2 sec.	69.1 min.
ResNet-56	56.9 sec.	132.8 hours	329.2 sec.	93.3 min.

utilization of CPU threads, as our training loop processes more images during each iteration compared to [15].

A limitation in finding the optimal trade-off between energy and accuracy is the dimension of the search space, which determines the search time and requires a carefully tuned search strategy. This problem is also found in mixed precision layer-wise quantization, in which the search space is q^{2L} , with q quantization levels for weights and activations, for L layers [11], [12]. Future work should focus on pruning the search space after a number of experiments (i.e., NSGA-II generations) to reduce its size, possibly reducing the time to converge. A further improvement over layer-wise approximation can be proposed by looking at past works on quantization. In AutoQ [3] channel-wise quantization is used to reduce the inference energy with less accuracy degradation than [11], [12], proving that NNs resilience to quantization errors has an intra-layer dependency besides the inter-layer one. Therefore, achieving an optimal energy-accuracy trade-off is possible by extending approximate computing in the channel dimension. In AutoQ [3], a bit-serial accelerator is required to support channel-wise quantization, whereas with MARLIN the only necessary modification, to enable it with the proposed RISC-V core, would be to adapt the CSR instructions inserted by our modified version of DORY. Nonetheless, the main challenge would be the efficient exploration of a wider search space.

V. CONCLUSION

In this paper, we presented MARLIN, a layer-wise approximation methodology leveraging a single multiplier architecture that can be configured runtime with 256 approximation levels to achieve an optimal trade-off between the inference energy and the task accuracy. In this work, a prototype based on a modified RISC-V core is proposed to test our methodology on a low-power IoT platform. The PULP toolchain has been adapted to automatically include the runtime approximation level selection alongside the instructions executed while processing convolutional layers. MARLIN can evaluate thousands of different NNs, leveraging NSGA-II to find the optimal configuration by generating a Pareto front that contains a set of layer-wise approximate NNs with reduced inference energy, without a significant accuracy loss.

REFERENCES

[1] M. Shafique, T. Theocharides, V. J. Reddy, and B. Murmann, "TinyML: Current progress, research challenges, and future roadmap," in *Proc. 58th ACM/IEEE Design Autom. Conf. (DAC)*, Nov. 2021, pp. 1303–1306.

[2] M. Merenda, C. Porcaro, and D. Iero, "Edge machine learning for AI-enabled IoT devices: A review," *Sensors*, vol. 20, no. 9, p. 2533, 2020.

[3] Q. Lou, F. Guo, M. Kim, L. Liu, and L. Jiang, "AutoQ: Automated kernel-wise neural network quantization," in *Proc. Int. Conf. Learn. Represent.*, 2020. [Online]. Available: <https://openreview.net/group?id=ICLR.cc/2020/Conference>

[4] N. Fafous et al., "AnaCoNGA: Analytical HW-CNN co-design using nested genetic algorithms," in *Proc. Design, Autom. Test Eur. Conf. Exhib. (DATE)*, Mar. 2022, pp. 238–243.

[5] A. Garofalo, M. Rusci, F. Conti, D. Rossi, and L. Benini, "PULP-NN: Accelerating quantized neural networks on parallel ultra-low-power RISC-V processors," *Phil. Trans. Roy. Soc. A, Math., Phys. Eng. Sci.*, vol. 378, no. 2164, Feb. 2020, Art. no. 20190155.

[6] A. Garofalo, G. Tagliavini, F. Conti, D. Rossi, and L. Benini, "XpulpNN: Accelerating quantized neural networks on RISC-V processors through ISA extensions," in *Proc. Design, Autom. Test Eur. Conf. Exhib. (DATE)*, Benin, Mar. 2020, pp. 186–191.

[7] T. Chen et al., "DianNao: A small-footprint high-throughput accelerator for ubiquitous machine-learning," in *Proc. Int. Conf. Architect. Support Program. Lang. Oper. Syst. (ASPLOS)*, Mar. 2014, pp. 269–284.

[8] Y. S. Shao et al., "Simba: Scaling deep-learning inference with multi-chip-module-based architecture," in *Proc. 52nd Annu. IEEE/ACM Int. Symp. Microarchitecture*, Oct. 2019, pp. 14–27.

[9] Y.-H. Chen, T. Krishna, J. Emer, and V. Sze, "Eyeriss: An energy-efficient reconfigurable accelerator for deep convolutional neural networks," *IEEE J. Solid-State Circuits*, vol. 52, no. 1, pp. 127–138, Jan. 2017.

[10] A. Parashar et al., "Timeloop: A systematic approach to DNN accelerator evaluation," in *Proc. IEEE Int. Symp. Perform. Anal. Syst. Softw. (ISPASS)*, Mar. 2019, pp. 304–315.

[11] K. Wang, Z. Liu, Y. Lin, J. Lin, and S. Han, "HAQ: Hardware-aware automated quantization with mixed precision," in *Proc. IEEE/CVF Conf. Comput. Vis. Pattern Recognit. (CVPR)*, Jun. 2019, pp. 8604–8612.

[12] N. Fafous et al., "HW-FlowQ: A multi-abstraction level HW-CNN co-design quantization methodology," *ACM Trans. Embedded Comput. Syst.*, vol. 20, no. 5s, pp. 1–25, Oct. 2021.

[13] H. Wu, P. Judd, X. Zhang, M. Isaev, and P. Micikevicius, "Integer quantization for deep learning inference: Principles and empirical evaluation," 2004, *arXiv:2004.09602*.

[14] H. Jiang, F. J. H. Santiago, H. Mo, L. Liu, and J. Han, "Approximate arithmetic circuits: A survey, characterization, and recent applications," *Proc. IEEE*, vol. 108, no. 12, pp. 2108–2135, Dec. 2020.

[15] V. Mrazek, Z. Vasicek, L. Sekanina, M. A. Hanif, and M. Shafique, "ALWANN: Automatic layer-wise approximation of deep neural network accelerators without retraining," in *Proc. IEEE/ACM Int. Conf. Comput.-Aided Design (ICCAD)*, Nov. 2019, pp. 1–8.

[16] X. He, W. Lu, G. Yan, and X. Zhang, "Joint design of training and hardware towards efficient and accuracy-scalable neural network inference," *IEEE J. Emerg. Sel. Topics Circuits Syst.*, vol. 8, no. 4, pp. 810–821, Dec. 2018.

[17] Z. G. Tasoulas, G. Zervakis, I. Anagnostopoulos, H. Amrouch, and J. Henkel, "Weight-oriented approximation for energy-efficient neural network inference accelerators," *IEEE Trans. Circuits Syst. I, Reg. Papers*, vol. 67, no. 12, pp. 4670–4683, Dec. 2020.

[18] Í. Taştan, M. Karaca, and A. Yurdakul, "Approximate CPU design for IoT end-devices with learning capabilities," *Electronics*, vol. 9, no. 1, p. 125, Jan. 2020.

[19] M. S. Ansari, V. Mrazek, B. F. Cockburn, L. Sekanina, Z. Vasicek, and J. Han, "Improving the accuracy and hardware efficiency of neural networks using approximate multipliers," *IEEE Trans. Very Large Scale Integr. (VLSI) Syst.*, vol. 28, no. 2, pp. 317–328, Feb. 2020.

[20] P. Jain, S. Huda, M. Maas, J. E. Gonzalez, I. Stoical, and A. Mirhoseini, "Learning to design accurate deep learning accelerators with inaccurate multipliers," in *Proc. Design, Autom. Test Eur. Conf. Exhib. (DATE)*, Mar. 2022, pp. 184–189.

[21] *PULP Platform*. Accessed: Jan. 23, 2023. [Online]. Available: <https://pulp-platform.org>

[22] M. Gautschi et al., "Near-threshold RISC-V core with DSP extensions for scalable IoT endpoint devices," *IEEE Trans. Very Large Scale Integr. (VLSI) Syst.*, vol. 25, no. 10, pp. 2700–2713, Oct. 2017.

[23] K. Deb, A. Pratap, S. Agarwal, and T. Meyarivan, "A fast and elitist multiobjective genetic algorithm: NSGA-II," *IEEE Trans. Evol. Comput.*, vol. 6, no. 2, pp. 182–197, Apr. 2002.

[24] M. Pinos, V. Mrazek, and L. Sekanina, "Prediction of inference energy on CNN accelerators supporting approximate circuits," in *Proc. 26th Int. Symp. Design Diag. Electron. Circuits Syst. (DDECS)*, May 2023, pp. 45–50.

- [25] E. Manor and S. Greenberg, "Using HW/SW codesign for deep neural network hardware accelerator targeting low-resources embedded processors," *IEEE Access*, vol. 10, pp. 22274–22287, 2022.
- [26] E. Manor and S. Greenberg, "Custom hardware inference accelerator for TensorFlow lite for microcontrollers," *IEEE Access*, vol. 10, pp. 73484–73493, 2022.
- [27] S. Venkataramani, A. Ranjan, K. Roy, and A. Raghunathan, "AxNN: Energy-efficient neuromorphic systems using approximate computing," in *Proc. IEEE/ACM Int. Symp. Low Power Electron. Design (ISLPED)*, Aug. 2014, pp. 27–32.
- [28] V. Mrazek, L. Sekanina, and Z. Vasicek, "Libraries of approximate circuits: Automated design and application in CNN accelerators," *IEEE J. Emerg. Sel. Topics Circuits Syst.*, vol. 10, no. 4, pp. 406–418, Dec. 2020.
- [29] E. Attoofian, "Increasing robustness against adversarial attacks through ensemble of approximate multipliers," in *Proc. IEEE Int. Conf. Netw., Archit. Storage (NAS)*, Oct. 2022, pp. 1–8.
- [30] A. Siddique and K. A. Hoque, "Is approximation universally defensive against adversarial attacks in deep neural networks?" in *Proc. Design, Autom. Test Eur. Conf. Exhib. (DATE)*, Mar. 2022, pp. 364–369.
- [31] *PyTorch*. Accessed: Mar. 11, 2023. [Online]. Available: <https://pytorch.org/>
- [32] F. Conti, "NEMO DNN quantization for deployment model," Eidgenössische Technische Hochschule Zürich (ETHZ), Università di Bologna (UNIBO), Tech. Rep., 2020.
- [33] D. Danopoulos, G. Zervakis, K. Siozios, D. Soudris, and J. Henkel, "AdaPT: Fast emulation of approximate DNN accelerators in PyTorch," *IEEE Trans. Comput.-Aided Design Integr. Circuits Syst.*, vol. 42, no. 6, pp. 2074–2078, Jun. 2023.
- [34] A. Burrello, A. Garofalo, N. Bruschi, G. Tagliavini, D. Rossi, and F. Conti, "DORY: Automatic end-to-end deployment of real-world DNNs on low-cost IoT MCUs," *IEEE Trans. Comput.*, vol. 70, no. 8, pp. 1253–1268, Aug. 2021.
- [35] L. Dadda, "Some schemes for parallel multipliers," *Alta Frequenza*, vol. 34, pp. 349–356, Jan. 1965.
- [36] C. R. Baugh and B. A. Wooley, "A two's complement parallel array multiplication algorithm," *IEEE Trans. Comput.*, vol. C-22, no. 12, pp. 1045–1047, Dec. 1973.
- [37] M. de la Guia Solaz, W. Han, and R. Conway, "A flexible low power DSP with a programmable truncated multiplier," *IEEE Trans. Circuits Syst. I, Reg. Papers*, vol. 59, no. 11, pp. 2555–2568, Nov. 2012.
- [38] T. Yang, T. Ukezono, and T. Sato, "A low-power high-speed accuracy-controllable approximate multiplier design," in *Proc. 23rd Asia South Pacific Design Autom. Conf. (ASP-DAC)*, Jan. 2018, pp. 605–610.
- [39] F.-Y. Gu, I.-C. Lin, and J.-W. Lin, "A low-power and high-accuracy approximate multiplier with reconfigurable truncation," *IEEE Access*, vol. 10, pp. 60447–60458, 2022.
- [40] A. G. M. Strollo, E. Napoli, D. De Caro, N. Petra, and G. D. Meo, "Comparison and extension of approximate 4–2 compressors for low-power approximate multipliers," *IEEE Trans. Circuits Syst. I, Reg. Papers*, vol. 67, no. 9, pp. 3021–3034, Sep. 2020.
- [41] M. Ha and S. Lee, "Multipliers with approximate 4–2 compressors and error recovery modules," *IEEE Embedded Syst. Lett.*, vol. 10, no. 1, pp. 6–9, Mar. 2018.
- [42] Z. Yang, J. Han, and F. Lombardi, "Approximate compressors for error-resilient multiplier design," in *Proc. IEEE Intl. Symp. Defect Fault Tolerance VLSI Nanotechnol. Syst.*, Oct. 2015, pp. 183–186.
- [43] K. He, X. Zhang, S. Ren, and J. Sun, "Deep residual learning for image recognition," in *Proc. IEEE Conf. Comput. Vis. Pattern Recognit. (CVPR)*, Jun. 2016, pp. 770–778.
- [44] A. Krizhevsky and G. Hinton, "Learning multiple layers of features from tiny images," Univ. Toronto, Toronto, ON, Canada, Tech. Rep., 2009. [Online]. Available: <https://www.cs.toronto.edu/~kriz/cifar.html>
- [45] L. N. Smith, "Cyclical learning rates for training neural networks," in *Proc. IEEE Winter Conf. Appl. Comput. Vis. (WACV)*, Mar. 2017, pp. 464–472.
- [46] J. Choi, Z. Wang, S. Venkataramani, P. I.-J. Chuang, V. Srinivasan, and K. Gopalakrishnan, "PACT: Parameterized clipping activation for quantized neural networks," 2018, *arXiv:1805.06085*.
- [47] E. Trommer, B. Waschneck, and A. Kumar, "High-throughput approximate multiplication models in PyTorch," in *Proc. 26th Int. Symp. Design Diag. Electron. Circuits Syst. (DDECS)*, May 2023, pp. 79–82.



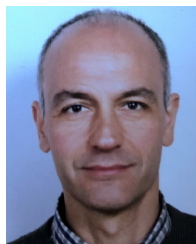
Flavia Guella (Student Member, IEEE) received the B.S. degree (summa cum laude) in electronics engineering from Università degli Studi di Palermo in 2020 and the M.S. degree (summa cum laude) in electronics engineering from Politecnico di Torino in 2023, where she is currently pursuing the Ph.D. degree in electronics and communications engineering, under the supervision of Prof. Maurizio Martina and Guido Masera. Her research interests include co-design methodologies for the efficient deployment of neural networks on low-power systems and approximate computing.



Emanuele Valpreda (Student Member, IEEE) received the B.S. and M.S. (summa cum laude) degrees in electronic and communications engineering from Politecnico di Torino in 2017 and 2019, respectively. He is currently pursuing the Ph.D. degree with the Electronics and Telecommunications Department, with a focus on energy-efficient neural network acceleration for edge computing, under the supervision of Prof. Maurizio Martina and Guido Masera. His current research interests include neural network compression, reliability, and approximate computing.



Michele Caon (Student Member, IEEE) received the B.S. and M.S. degrees (summa cum laude) from Politecnico di Torino in 2017 and 2019, respectively, where he is currently pursuing the Ph.D. degree with the Electronics and Telecommunications Department, under the supervision of Prof. Maurizio Martina and Guido Masera. His research interests include innovative digital, integrated, and programmable computing circuits and systems. He is currently working on near-memory computing circuits embedded in heterogeneous systems-on-chip.



Guido Masera (Senior Member, IEEE) received the Dr.-Ing. (summa cum laude) and Ph.D. degrees in electronic engineering from Politecnico di Torino, Italy. He has been a Professor with the Electronics and Telecommunications Department, Politecnico di Torino, since 1992. His research interests include several aspects of the design of digital integrated circuits and systems, with a special emphasis on high-performance architectures for communications, forward error correction, image and video coding, cryptography, and hardware accelerators for machine

learning. He has more than 200 publications and two patents. He was a designer of several ASIC components. He is an Associate Editor of *Electronics* (MDPI) and a Former Associate Editor of IEEE TRANSACTIONS ON CIRCUITS AND SYSTEMS—I: REGULAR PAPERS, IEEE TRANSACTIONS ON CIRCUITS AND SYSTEMS—II: EXPRESS BRIEFS, and *IET Circuits, Devices and Systems*.



Maurizio Martina (Senior Member, IEEE) received the Dr.-Ing. and Ph.D. degrees in electronic engineering and electronic and communications engineering from Politecnico di Torino, Italy, in 2000 and 2004, respectively. He has been a Professor with the Electronics and Telecommunications Department, Politecnico di Torino, since 2014. He has more than 100 publications and holds two patents. His research interests include computer architecture and VLSI design of digital integrated circuits for image and video coding, forward error correction, cryptography, and artificial intelligence. He served as an Associate Editor for IEEE TRANSACTIONS ON CIRCUITS AND SYSTEMS—I: REGULAR PAPERS and as a Guest Editor for several special issues, including BioCAS 2017 Special Issue of IEEE TRANSACTIONS OF BIOMEDICAL CIRCUITS AND SYSTEMS AND ISCAS 2023 Special Issue of IEEE TRANSACTIONS ON CIRCUITS AND SYSTEMS—II: EXPRESS BRIEFS. He has been part of the Organizing and Technical Committee of several IEEE conferences, including BioCAS 2017, AICAS 2020, and PRIME 2023.